

Direct observation of ground-state lactam–lactim tautomerization using temperature-jump transient 2D IR spectroscopy

Chunte Sam Peng, Carlos R. Baiz, and Andrei Tokmakoff^{1,2}

Department of Chemistry, Massachusetts Institute of Technology, Cambridge, MA 02139

Edited by Peter Hamm, University of Zurich, Zurich, Switzerland, and accepted by the Editorial Board April 19, 2013 (received for review February 19, 2013)

We provide a systematic characterization of the nanosecond ground-state lactam–lactim tautomerization of pyridone derivatives in aqueous solution under ambient conditions using temperature-jump transient 2D IR spectroscopy. Although electronic excited-state tautomerization has been widely studied, experimental work on the ground electronic state, most relevant to chemistry and biology, is lacking. Using 2D IR spectroscopy, lactam and lactim tautomers of 6-chloro-2-pyridone and 2-chloro-4-pyridone are unambiguously identified by their unique cross-peak patterns. Monitoring the correlated exponential relaxation of these signals in response to a laser temperature jump provides a direct measurement of the nanosecond tautomerization kinetics. By studying the temperature, concentration, solvent, and pH dependence, we extract a thermodynamic and kinetic characterization and conclude that the tautomerization proceeds through a two-state concerted mechanism. We find that the intramolecular proton transfer is mediated by bridging water molecules and the reaction barrier is dictated by the release of a proton from pyridone, as would be expected for an efficient Grothuss-type proton transfer mechanism.

keto-enol tautomerism | multidimensional | time-resolved spectroscopy | ultrafast

Tautomerism of aromatic heterocycles has been extensively studied owing to its importance in biochemical processes such as enzyme catalysis (1), ligand binding (2), and spontaneous mutagenesis (3). To characterize the tautomeric equilibria, researchers have used techniques such as UV absorption (4), circular dichroism (5), X-ray crystallography (3), NMR (6), Raman (7), and IR absorption spectroscopy (8). However, these methods face several challenges to characterizing thermodynamic and kinetic data for tautomeric equilibria and exchange processes. For example, electronic spectra are broad and featureless, which complicates spectral interpretation, particularly for systems with multiple tautomers. Although NMR provides excellent structural resolution, it can only directly monitor chemical exchange in real time on millisecond and longer time scales, rather than the picosecond to nanosecond time scales expected for proton transfer under physiological conditions. From the theoretical point of view, quantum mechanical calculations have been performed extensively to characterize the relative stability of tautomeric systems, their activation barriers, and the reaction mechanisms (9, 10); nevertheless, experimental validation of these predictions is scarce. To provide a characterization under ambient aqueous conditions, we need a technique with both the structural sensitivity to unambiguously identify various tautomers and the time resolution to probe the rapid proton transfer dynamics. To this end, we demonstrate the capability of 2D IR spectroscopy coupled with a nanosecond temperature-jump (T-jump) laser to reveal the nonequilibrium lactam–lactim tautomerization kinetics of pyridone derivatives.

Time-resolved studies of tautomerism have a long and storied history. In the 1960s, Manfred Eigen pioneered the T-jump relaxation method using rapid electrical heating in electrolyte solutions to trigger fast chemical reactions, such as the recombination of the enolate ion with H⁺ to form either a keto or enol tautomer

(11). Others have since used a similar approach, using a T-jump monitored by UV absorption, to study tautomerism of small molecules on the microsecond time scale (12–14). These ground-breaking experiments provided the early insights into proton transfer and tautomerization kinetics. However, they still suffer from certain limitations, including the difficulty of interpreting variations in electronic spectra, the inclusion of pH indicators, and questions about reactive species that may be created by the capacitive discharge. The more recent studies to capture proton transfer dynamics have used ultrafast photo-excitation to induce tautomerization on the excited electronic state (15–20). This has proven a fruitful test bed for dynamics, but experiments in room-temperature aqueous solution would more accurately report on physiological tautomerism.

Two-dimensional IR spectra, analogous to 2D NMR, exhibit cross-peak patterns between vibrational modes that provide distinct signatures of molecular structures, although with subpicosecond time resolution (21). Previously, we have shown that intramolecular couplings between the vibrational modes of aromatic heterocycles result in pronounced 2D IR cross-peaks (22), and therefore the lactam and lactim tautomers of 2-pyridone derivatives can be differentiated based on the distinct cross-peak patterns from individual species (23). Our interest is to make use of 2D IR to explore the time scale and mechanism for tautomer exchange. Chemical exchange processes at equilibrium have been characterized through waiting-time 2D IR experiments in which the delay between the excitation and detection pulses is varied (24). Nevertheless, the time window for these experiments is limited to the vibrational lifetime of the systems, typically a few picoseconds. To circumvent this limitation, one can perform transient 2D IR (t-2D IR) experiments that follow reequilibration after an abrupt perturbation (25–30). Our strategy to monitor ground-state reactivity is to perform t-2D IR triggered by a nanosecond T-jump and observe the tautomeric interconversion in real time during the reequilibration. In the following, we report the nanosecond lactam–lactim tautomerization kinetics of pyridone derivatives in deuterated water (D₂O) and find that tautomerization proceeds through a concerted intramolecular proton transfer facilitated by bridging water molecules. This approach opens up an opportunity to study tautomerization under physiological conditions and provides a platform for experimental validation of electronic structure models that offer an atomistic picture of the barrier-crossing processes.

Author contributions: C.S.P. and A.T. designed research; C.S.P. and C.R.B. performed research; C.S.P. analyzed data; and C.S.P., C.R.B., and A.T. wrote the paper.

The authors declare no conflict of interest.

This article is a PNAS Direct Submission. P.H. is a guest editor invited by the Editorial Board.

¹Present address: Department of Chemistry and The James Frank Institute, University of Chicago, Chicago, IL 60637.

²To whom correspondence should be addressed. E-mail: tokmakoff@uchicago.edu.

This article contains supporting information online at www.pnas.org/lookup/suppl/doi:10.1073/pnas.1303235110/-DCSupplemental.

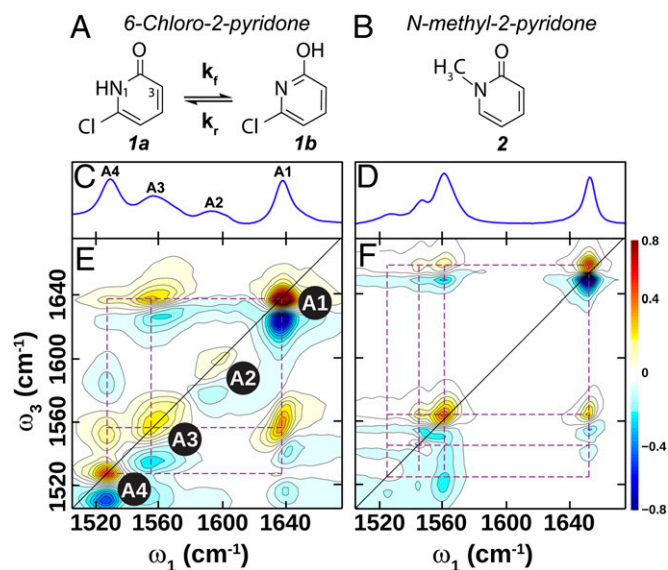


Fig. 1. Chemical structures (A and B), equilibrium FTIR (C and D), and 2D IR spectra (E and F) with ZZZZ polarization for 6-chloro-2-pyridone at 40 °C (Left) and *N*-methyl-2-pyridone at 25 °C (Right). The dashed grids show the coupled vibrations from the lactam tautomers. Two-dimensional IR spectra are plotted with 21 equally spaced contours between ± 0.8 of the maximum intensity.

Results and Discussion

Equilibrium Measurements. Because of its simple structure and similarity to DNA bases, 2-pyridone has drawn considerable interest and is regarded as the prototype molecule to study lactam–lactim tautomerization. It is known that in aqueous solution 2-pyridone exists primarily in the lactam form, and the addition of chlorine at the 6-position significantly shifts the tautomeric equilibrium toward the lactim form (14). The structure, FTIR, and 2D IR spectrum of 6-chloro-2-pyridone at 40 °C in D₂O is shown in Fig. 1. In an absorptive 2D IR spectrum, peaks appear as a doublet with a positive peak (red) originating from the ground to first excited vibrational state (0–1) transition, and a negative peak (blue) owing to the 1–2 transition. The diagonal features, labeled A1–A4, can be mapped to the corresponding peaks in the linear absorption spectrum, whereas the cross-peaks correlate the vibrational excitation (ω_1) and detection (ω_3) frequencies, which allow the separation of different chemical species in a mixture, even with

significant spectral congestion. Peak A1 is the carbonyl stretch of the lactam form (**1a**), and peaks A3 and A4 are ring vibrations of the same species, indicated by their pronounced cross-peaks to A1 (23). Peak A2, which does not have cross-peaks with A1, A3, and A4, arises from the ring vibration of the lactim tautomer (**1b**), coupled to D₂O bending motions. These peak assignments are further validated by comparing to the 2D IR spectrum of *N*-methyl-2-pyridone (**2**, Fig. 1B), whose labile proton has been replaced by a methyl group to block tautomerization. The 2D IR spectrum of **2** closely resembles the spectral features of **1a** (indicated by the dashed purple lines), except for the extra ring mode and the absolute peak frequencies. Previous 2D IR studies of the lactam–lactim tautomerization of **1** were used to determine the equilibrium constant $K_{eq} = [1b]/[1a] = 0.53 \pm 0.02$ at 25 °C and found that this value increases with temperature (23).

Transient 2D IR Spectroscopy. We performed T-jump IR experiments using the methods described in refs. 31–33 to probe time-dependent changes to the tautomer populations. Briefly, we used 11-mJ pulses at $\lambda = 2 \mu\text{m}$ from a 20-Hz neodymium-doped yttrium aluminum garnet (Nd:YAG) pumped optical parametric oscillator to excite the O–D stretch overtone of D₂O, raising the temperature of the solution by 10° within the 5-ns pulse duration. Electronically synchronized femtosecond mid-IR pulse sequences following the T-jump pulse were used to measure the change in a nonlinear signal. We recorded the difference signal relative to a reference spectrum, $\Delta S(\tau, T) = S(\tau, T) - S(T_i)$, where τ is the time delay between the T-jump and 2D IR pulses and $S(T_i)$ is the equilibrium spectrum measured before the T-jump. Tautomeric interconversion was monitored with t-2D IR and transient heterodyne-detected dispersed vibrational echo (t-HDVE). Transient HDVE was performed with fixing the excitation at 0 fs and the waiting time at 150 fs. The complex-value t-HDVE signal was measured by Fourier-transform spectral interferometry, and its information content is equivalent to the projection of the t-2D IR spectrum onto the detection frequency axis. Although t-2D IR spectra provide the most information on the system, the measurement requires roughly 100 times longer sampling time than t-HDVE. Therefore, we assigned the transient spectral features using full t-2D IR spectra at selected time delays and obtained kinetics from the more finely sampled one-dimensional t-HDVE spectra.

Transient 2D IR and the corresponding t-HDVE spectra of **1** in phosphate-buffered D₂O at pD (acidity in D₂O) 7.8 starting from an initial temperature $T_i = 40 \text{ °C}$ are displayed in Figs. 2 and 3B, respectively. We use different color maps for the equilibrium and transient spectra to emphasize that t-2D IR spectra are time-dependent difference spectra with respect to the equilibrium spectra

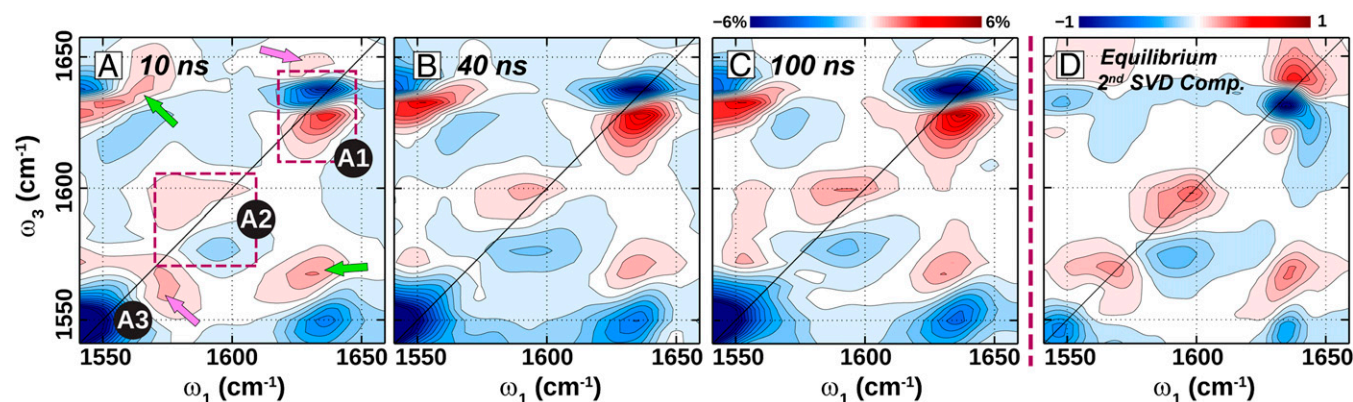


Fig. 2. Transient difference 2D IR spectra at T-jump delays of 10 ns (A), 40 ns (B), and 100 ns (C) for **1** following a T-jump from 40 to 50 °C. These spectra are plotted between $\pm 6\%$ difference signal relative to the equilibrium spectrum. (D) Normalized second-component spectrum calculated from the SVD analysis of the temperature-dependent 2D IR spectra from 10 °C to 80 °C, modified from ref. 23. The frequency axes are plotted differently from Fig. 1 to focus on the growth of the lactim peak.

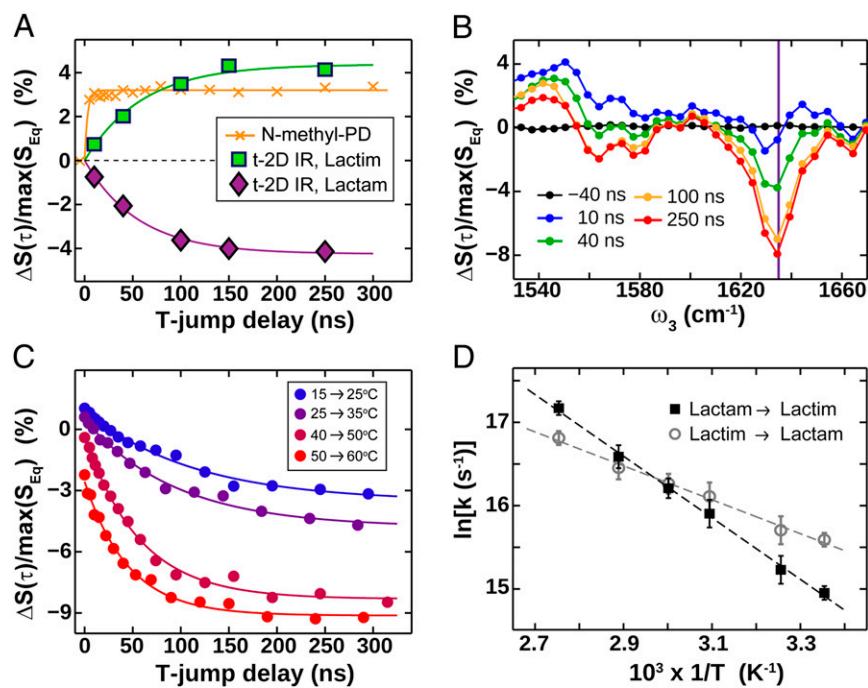


Fig. 3. (A) Integrated peak intensities of the t-2D IR absolute value spectra for **1** at $T_i = 40^\circ\text{C}$. The integration regions for lactim and lactam are shown by the green and magenta boxes in Fig. S1, at $\sim 1,600\text{ cm}^{-1}$ and $\sim 1,640\text{ cm}^{-1}$, respectively. The t-2D IR amplitudes have been scaled to be better compared with the t-HDVE traces (the error bars are smaller than the marker size; Fig. S1). The solid lines are the single exponential fits. The orange crosses display the t-HDVE time trace for **2** at $\omega_3 = 1,649\text{ cm}^{-1}$ at $T_i = 25^\circ\text{C}$. (B) Transient difference spectra derived from the absolute value of the complex value t-HDVE for **1** from 40 to 50°C at selected T-jump delays. (C) Representative t-HDVE time traces at selected T_i for the C=O stretch of **1** at $\omega_3 = 1,634\text{ cm}^{-1}$. (D) The Arrhenius plot showing the temperature dependence of the relaxation rate.

at T_i . A loss of population appears in t-2D IR difference spectra as a negative (blue) peak on the top with a positive (red) peak on the bottom. At 10 ns following the T-jump, a bleach of the C=O stretch of **1a** at $1,634\text{ cm}^{-1}$ is observed (box A1 in Fig. 2A). Moreover, a gain feature (red above and blue below the diagonal) is identified for peak A2, which is a ring vibrational mode of **1b**. These spectral changes indicate the growth of lactim tautomer **1b** at the expense of the lactam tautomer **1a**. Here a 10° temperature change corresponds to an equilibrium population drop of **1a** from 59 to 55%. Both the A1 loss and the A2 gain increase with T-jump delay, as illustrated in Fig. 3A by the integrated peak intensities obtained from the t-2D IR absolute value spectra (Fig. S1). We fit both time traces to monoexponential decays with relaxation time constants of 56 ns and 60 ns for **1a** and **1b**, respectively. The nonstretched exponential behavior and the common time constant provide experimental evidence for two-state tautomerization kinetics and a concerted proton transfer mechanism without a long-lived intermediate state.

The loss of the lactam C=O stretch is also observed in the t-HDVE spectra as a negative difference signal marked by the purple line in Fig. 3B. A single exponential decay with a time constant of $56 \pm 9\text{ ns}$ was measured for this T-jump response at $T = 40 \rightarrow 50^\circ\text{C}$ (Fig. 3C), which is in excellent agreement with the kinetics obtained from t-2D IR. Considering that t-HDVE can be collected much faster than t-2D IR to allow more accurate kinetic measurements, in the following discussion we used the A1 response from t-HDVE to represent the kinetics of both the loss of **1a** and gain of **1b**. We note, however, owing to significant spectral congestion in this frequency region, the gain of the lactim tautomer cannot be readily identified in t-HDVE. In contrast to the clear gain feature at $\sim 1,600\text{ cm}^{-1}$ observed in the t-2D IR spectra, t-HDVE exhibits only a small positive peak on top of the broad loss features from A1 and A3. The ability to resolve both tautomeric species in t-2D IR spectra demonstrates the increased spectral information content available in 2D IR spectra compared with the equivalent one-dimensional representations.

To verify that the observed response corresponds to tautomerization, and rule out any T-jump artifacts such as cavitation or thermally induced change in dielectric constants (34), we carried out a negative control experiment on **2**, whose N1

tautomerization site has been blocked. The t-HDVE time trace of the C=O stretch of **2** is plotted as orange crosses in Fig. 3A (spectra shown in Fig. S2). Only a T-jump pulse-width limited baseline shift that results from increased solvent transmission was observed, confirming that the nanosecond exponential relaxation is due to the lactam–lactim tautomerization.

In addition to reporting on the tautomeric interconversion, t-2D IR provides spectral signatures of the solvent environment. In the 10-ns spectrum, positive features (violet arrows in Fig. 2A) appear on the blue side of the A1 and A3 modes—a sign of a blue-shift of the peak, which suggests weakening or loss of hydrogen bonds (HBs) to **1a** (23). The more complicated line-shapes of the A1/A3 cross-peaks (green arrows) are interpreted as a convolution between the blue-shifts and the population decrease of **1a** (Fig. S3 gives more details). At longer T-jump delays, most of the spectral changes are solely due to the tautomeric interconversion, indicating that the solvent HB equilibration is finished by $\sim 10\text{ ns}$. Overall, these changes in the t-2D IR spectra are encapsulated in the second spectral component from the singular value decomposition (SVD) analysis of the temperature-dependent equilibrium 2D IR spectra from 10°C to 80°C (Fig. 2D).

Temperature Dependence. To determine the thermodynamic properties of tautomerization, we monitored the time evolution of A1 from the t-HDVE spectra at different initial temperatures (Fig. 3C). With increasing temperature, the relaxation rate speeds up and the amplitude of the difference signal increases. First-order kinetics for the two-state exchange leads to an observed relaxation rate of $k_{obs} = 1/\tau_{obs} = k_f + k_r$, where τ_{obs} is the observed relaxation time constant and k_f and k_r are the forward and reverse rate constants, respectively. Using the equilibrium constant $K_{eq} = [\mathbf{1b}]/[\mathbf{1a}] = k_f/k_r$ (23), k_f and k_r can be determined at each temperature. The temperature dependence of k_f and k_r (Fig. 3D) was used to extract the activation barrier E_a and preexponential factors A for these reactions (Table 1). We obtained an activation barrier of $7.4 \pm 0.5\text{ kcal/mol}$ ($\sim 12\text{ k}_B\text{T}$) for the lactam-to-lactim tautomerization. This can be compared with the calculated results for the parent molecule 2-pyridone, using density functional theory (DFT) and second-order Møller–Plesset perturbation theory electronic-structure methods by Sonnenberg et al. (10). The energy barrier was found to be

Table 1. Thermodynamic and kinetic fit parameters obtained for 6-chloro-2-pyridone and 2-chloro-4-pyridone at temperatures of 25 °C and 30 °C, respectively

Molecule	Reaction	k , 10^6 s^{-1}	A , s^{-1}	E_a , kcal/mol	ΔH^\ddagger , kcal/mol	ΔS^\ddagger , cal/mol·K	ΔH , kcal/mol	ΔS , cal/mol·K
6-chloro-2-pyridone	Lactam \rightarrow lactim	3.1 ± 0.1	$8.2 \pm 0.3 \times 10^{11}$	7.4 ± 0.5	6.7 ± 0.5	-6.4 ± 0.2	3.3 ± 0.1	9.8 ± 0.2
	Lactim \rightarrow lactam	5.9 ± 0.2	$6.0 \pm 0.2 \times 10^9$	4.1 ± 0.5	3.4 ± 0.5	-16.2 ± 0.8		
2-chloro-4-pyridone	Lactam \rightarrow lactim	10.2 ± 2.5	$1.8 \pm 0.5 \times 10^{13}$	8.7 ± 0.6	8.1 ± 0.6	0.1 ± 0.0	3.9 ± 0.1	15.3 ± 0.4
	Lactim \rightarrow lactam	3.2 ± 0.8	$8.6 \pm 2.2 \times 10^9$	4.8 ± 0.6	4.1 ± 0.6	-15.2 ± 0.9		

~40 kcal/mol in isolation, and further reduced to ~15 kcal/mol with the addition of one explicit water molecule to mediate the proton transfer. The microsolvation configuration of pyridone used in their calculation is similar to the structure (Fig. S4) that gives reasonable agreement between the experimental and calculated IR absorption spectra (23). It is not surprising that the calculated E_a for 2-pyridone is higher than the experimental value for 6-chloro-2-pyridone because the chlorine substitution significantly lowers the relative energy of the lactim tautomer. Additionally, it has not been established that a specific computational method can accurately predict the energetics of a tautomeric system. Most importantly, the significant reduction in the activation energy by hydrating water molecules argues strongly for a solvent-mediated tautomerization mechanism in our experiments.

We stress again that our experiments probe the rare tautomerization events on the ground-electronic state, in contrast to excited-state proton transfer (ESPT). Electronic excitation reduces $\text{p}K_a$, reshapes the energy surface, and lowers the tautomerization barrier, thus leading to much faster proton transfer rates than in the ground state (15). For example, photo-initiated ESPT in 7-azaindole/alcohol complexes occurs within ~100 ps with negligible barrier (<1 kcal/mol) (17), and the double-proton transfer in 7-azaindole dimer proceeds with a 1.1-ps time constant (18).

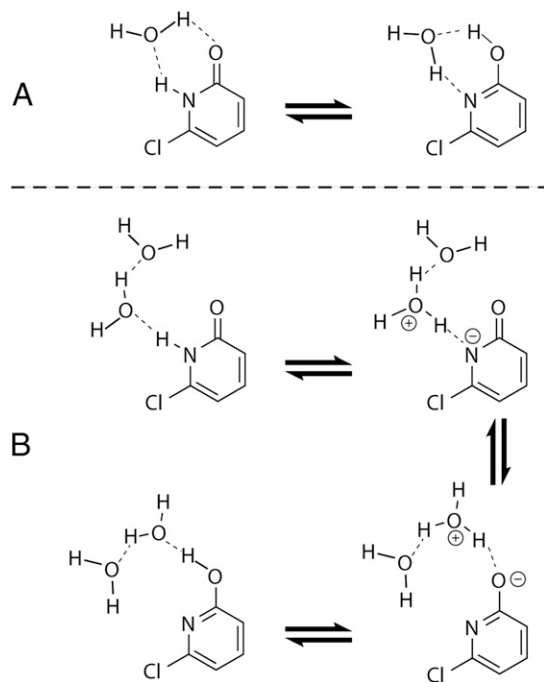
We also calculated the activation enthalpy and entropy (Table 1) using linear fits to the Eyring–Polanyi equation $\ln(k/T) = -\Delta H^\ddagger/RT + \Delta S^\ddagger/R + \ln(k_B/h)$. Because the internal entropies of the two tautomeric forms are not expected to differ significantly, the negative ΔS^\ddagger observed suggests that the transition state involves a well-structured solvation complex, for instance a water wire or ring structure between the solute and the solvating water molecules. Both the small activation barrier and negative activation entropy suggest the presence of bridging water molecules during tautomerization.

Solvent Dependence. To explore the involvement of the solvent, we measured the relaxation rates in different EtOD/D₂O solvent mixtures at $T_i = 25 \text{ °C}$ (Fig. S5). We found that the rate dropped by a factor of 1.8 when the D₂O volume percentage decreased from 100 to 40%, even though the viscosity of ethanol/water mixtures exhibits a maximum at 0.25 mol fraction of ethanol (35). This observation suggests that the dense hydrogen-bonding network of water may play an important role in facilitating tautomerization. Even though the exact nature of the solvent effect on tautomerization requires further investigation, our present study is not consistent with tautomerism via intramolecular proton transfer without solvent mediation, which has been observed for protonated uracil in the gas phase (36) and suggested for glycine using NMR relaxation methods (37).

2-Chloro-4-Pyridone. Several tautomerization mechanisms have been proposed. For example, intermolecular double-proton tunneling has been suggested for the spontaneous formation of enol tautomers in Watson–Crick base pairs (38) and has been observed for imidazole and pyrazole in nonaqueous solvents at -100 °C (39). We precluded the possibility of dimer formation in water because both the FTIR spectra (23) and T-jump relaxation rates (Fig. S6) were found to be concentration-independent. Alternatively, intramolecular proton transfer with water participation can proceed via a concerted (Fig. 4A) or a stepwise (Fig. 4B) mechanism. The stepwise mechanism, also referred to as “dissociative” mechanism,

involves an ionic intermediate in which the nitrogen proton becomes solvated. The excess proton can then diffuse or undergo an undirected Grothuss transport to the proton acceptor site. However, proton transfer by concerted tautomerization mostly likely proceeds as a Grothuss transfer with the assistance of a water bridge.

Diffusive proton transfer or direct intramolecular tunneling should be strongly influenced by changes in proximity between proton acceptor and donor sites. We tested this by measuring the T-jump relaxation rates for 2-chloro-4-pyridone (**3a**, structure shown in Fig. 5B), in which the carbonyl and N-D groups are in the *para* position—as opposed to *ortho* position in **1a**. Temperature-dependent FTIR of **3** at $\text{pD} = 7.8$ (Fig. 5A) shows that the C=O intensity at $1,626 \text{ cm}^{-1}$ decreases whereas the $1,581\text{-cm}^{-1}$ peak increases with temperature. The equilibrium 2D IR spectrum of **3** (Fig. 5C) reveals that these two peaks are from two separate species, which we attribute to the lactam and lactim tautomers based on DFT calculations and the similarities to the spectra of **1**. We obtained the T-jump relaxation rates through the loss of the C=O peak measured with the t-HDVE spectra (Fig. S7). The relaxation time constant measured under the same conditions ($\text{pD} = 7.8$, $T_i = 40 \text{ °C}$) for **3** was $49 \pm 13 \text{ ns}$, which is slightly faster than that of **1**. We calculated the activation thermodynamic parameters using the temperature dependence of the relaxation rates (Fig. 5D and Table 1) and found that they are within 2 kcal/mol of those of **1**. The similar kinetics of **1** and **3** exclude the possibility of intramolecular tunneling because the distance

**Fig. 4.** Possible mechanisms for the tautomerization of **1**. (A) Concerted mechanism with water-bridge facilitating the proton transfer. Longer bridging networks are possible. (B) Stepwise tautomerization through ionic intermediates, catalyzed by water molecules.

a capacitive discharge and that 2D IR spectroscopy offers substantive structural information and direct probing of the molecules of interest.

Conclusion

In conclusion, we have used the T-jump transient 2D IR spectroscopy to provide an in-depth characterization of the ground-state lactam–lactim tautomerization of pyridone derivatives in aqueous solution under ambient conditions. Using the distinctive cross-peak patterns, we can clearly distinguish the tautomeric forms. We track the time evolution of the lactam carbonyl peak following the T-jump to obtain the kinetics and calculate the activation thermodynamic variables. The concentration independence of the T-jump relaxation rate rules out the tautomerization mechanism via dimerization. The time constants of the single exponential t-2D IR signals of the lactam loss and lactim gain are nearly identical, indicating that the tautomerization proceeds through a two-state, concerted mechanism without a long-lived intermediate species. The comparison between the two pyridone derivatives, the solvent dependence, and the pD dependence preclude intramolecular tunneling and strongly

support proton transfer in water wires following a Grotthuss mechanism. We concluded that tautomerization of pyridone derivatives in water proceeds via the two-state concerted, and nondissociative, mechanism and that the rate-limiting step is the release of proton into the solvating water environment.

Materials and Methods

Chemicals were purchased from Sigma-Aldrich and dissolved in phosphate buffer in D₂O. The pD was adjusted with DCl and NaOD. Samples were filtered with an ultrafiltration tube to reduce scatter and the propensity of T-jump cavitation effects (34). Two-dimensional IR spectroscopy experiments were performed following procedures described in detail in [Supporting Information](#) and refs. 31 and 33.

ACKNOWLEDGMENTS. We thank Mike Reppert and Kevin C. Jones for stimulating discussions. This work was supported by National Science Foundation Grant CHE-1212557, the Massachusetts Institute of Technology (MIT) Center for Environmental Health Sciences [National Institutes of Health (NIH) Center Grant P30-ES002109], the MIT Laser Biomedical Research Center (NIH Center Grant P41-EB015871), and Agilent Technologies. C.R.B. acknowledges support from Ruth L. Kirschstein National Research Service Award F32GM105104.

- Vila JA, Arnautova YA, Vorobjev Y, Scheraga HA (2011) Assessing the fractions of tautomeric forms of the imidazole ring of histidine in proteins as a function of pH. *Proc Natl Acad Sci USA* 108(14):5602–5607.
- Thore S, Leibundgut M, Ban N (2006) Structure of the eukaryotic thiamine pyrophosphate riboswitch with its regulatory ligand. *Science* 312(5777):1208–1211.
- Wang W, Hellinga HW, Beese LS (2011) Structural evidence for the rare tautomer hypothesis of spontaneous mutagenesis. *Proc Natl Acad Sci USA* 108(43):17644–17648.
- Beak P (1977) Energies and alkylations of tautomeric heterocyclic compounds: Old problems — new answers. *Acc Chem Res* 10(5):186–192.
- Nemeria NS, Chakraborty S, Balakrishnan A, Jordan F (2009) Reaction mechanisms of thiamin diphosphate enzymes: Defining states of ionization and tautomerization of the cofactor at individual steps. *FEBS J* 276(9):2432–2446.
- Balakrishnan A, Paramasivam S, Chakraborty S, Polenova T, Jordan F (2012) Solid-state nuclear magnetic resonance studies delineate the role of the protein in activation of both aromatic rings of thiamin. *J Am Chem Soc* 134(1):665–672.
- Suen W, Spiro TG, Sowers LC, Fresco JR (1999) Identification by UV resonance Raman spectroscopy of an imino tautomer of 5-hydroxy-2'-deoxycytidine, a powerful base analog transition mutagen with a much higher unfavored tautomer frequency than that of the natural residue 2'-deoxycytidine. *Proc Natl Acad Sci USA* 96(8):4500–4505.
- Miles HT (1961) Tautomeric forms in a polynucleotide helix and their bearing on the structure of DNA. *Proc Natl Acad Sci USA* 47:791–802.
- Colominas C, Luque FJ, Orozco M (1996) Tautomerism and protonation of guanine and cytosine. Implications in the formation of hydrogen-bonded complexes. *J Am Chem Soc* 118(29):6811–6821.
- Sonnenberg JL, Wong KF, Voth GA, Schlegel HB (2009) Distributed Gaussian valence bond surface derived from ab initio calculations. *J Chem Theory Comput* 5(4):949–961.
- Eigen M, Ilgenfritz G, Kruse W (1965) Eine kinetische Methode zur Untersuchung schneller prototroper Tautomerisierungsreaktionen. *Chem Ber* 98(5):1623–1638.
- Dreyfus M, Dodin G, Bensaude O, Dubois JE (1975) Tautomerism of purines. I. N(7)H in equilibrium N(9)H equilibrium in adenine. *J Am Chem Soc* 97(9):2369–2376.
- Stuehr J (1967) Kinetics of proton transfer and tautomerism in aqueous diacetylacetone. A temperature-jump investigation. *J Am Chem Soc* 89(12):2826–2832.
- Bensaude O, Dreyfus M, Dodin G, Dubois JE (1977) Intramolecular nondissociative proton transfer in aqueous solutions of tautomeric heterocycles: A temperature-jump kinetic study. *J Am Chem Soc* 99(13):4438–4446.
- Demchenko AP, Tang KC, Chou PT (2013) Excited-state proton coupled charge transfer modulated by molecular structure and media polarization. *Chem Soc Rev* 42(3):1379–1408.
- Douhal A, Kim SK, Zewail AH (1995) Femtosecond molecular dynamics of tautomerization in model base pairs. *Nature* 378(6554):260–263.
- Kwon O-H, Lee Y-S, Park HJ, Kim Y, Jang D-J (2004) Asymmetric double proton transfer of excited 1:1 7-azaindole/alcohol complexes with anomalously large and temperature-independent kinetic isotope effects. *Angew Chem Int Ed Engl* 43(43):5792–5796.
- Takeuchi S, Tahara T (2007) The answer to concerted versus step-wise controversy for the double proton transfer mechanism of 7-azaindole dimer in solution. *Proc Natl Acad Sci USA* 104(13):5285–5290.
- Dupradeau F-Y, Case DA, Yu C, Jimenez R, Romesberg FE (2005) Differential solvation and tautomer stability of a model base pair within the minor and major grooves of DNA. *J Am Chem Soc* 127(44):15612–15617.
- Laermer F, Elsaesser T, Kaiser W (1988) Femtosecond spectroscopy of excited-state proton transfer in 2-(2'-hydroxyphenyl)benzothiazole. *Chem Phys Lett* 148(2–3):119–124.
- Hamm P, Zanni MT (2011) *Concepts and Methods of 2D Infrared Spectroscopy* (Cambridge Univ Press, Cambridge, UK).
- Peng CS, Jones KC, Tokmakoff A (2011) Anharmonic vibrational modes of nucleic acid bases revealed by 2D IR spectroscopy. *J Am Chem Soc* 133(39):15650–15660.
- Peng CS, Tokmakoff A (2012) Identification of lactam–lactim tautomers of aromatic heterocycles in aqueous solution using 2D IR spectroscopy. *J Phys Chem Lett* 3(22):3302–3306.
- Fayer MD (2009) Dynamics of liquids, molecules, and proteins measured with ultrafast 2D IR vibrational echo chemical exchange spectroscopy. *Annu Rev Phys Chem* 60(1):21–38.
- Hamm P, Helbing J, Bredenbeck J (2008) Two-dimensional infrared spectroscopy of photoswitchable peptides. *Annu Rev Phys Chem* 59:291–317.
- Kolano C, Helbing J, Kozinski M, Sander W, Hamm P (2006) Watching hydrogen-bond dynamics in a beta-turn by transient two-dimensional infrared spectroscopy. *Nature* 444(7118):469–472.
- Anna JM, Baiz CR, Ross MR, McCanne R, Kubarych KJ (2012) Ultrafast equilibrium and non-equilibrium chemical reaction dynamics probed with multidimensional infrared spectroscopy. *Int Rev Phys Chem* 31(3):367–419.
- Chung HS, Ganim Z, Jones KC, Tokmakoff A (2007) Transient 2D IR spectroscopy of ubiquitin unfolding dynamics. *Proc Natl Acad Sci USA* 104(36):14237–14242.
- Jones KC, Peng CS, Tokmakoff A (2013) Folding of a heterogeneous β -hairpin peptide from temperature-jump 2D IR spectroscopy. *Proc Natl Acad Sci USA* 110(8):2828–2833.
- Xiong W, et al. (2009) Transient 2D IR spectroscopy of charge injection in dye-sensitized nanocrystalline thin films. *J Am Chem Soc* 131(50):18040–18041.
- Chung HS, Khalil M, Smith AW, Tokmakoff A (2007) Transient two-dimensional IR spectrometer for probing nanosecond temperature-jump kinetics. *Rev Sci Instrum* 78(6):063101.
- Jones KC, Ganim Z, Tokmakoff A (2009) Heterodyne-detected dispersed vibrational echo spectroscopy. *J Phys Chem A* 113(51):14060–14066.
- Jones KC, Ganim Z, Peng CS, Tokmakoff A (2012) Transient two-dimensional spectroscopy with linear absorption corrections applied to temperature-jump two-dimensional infrared. *J Opt Soc Am B* 29(1):118–129.
- Wray WO, Aida T, Dyer RB (2002) Photoacoustic cavitation and heat transfer effects in the laser-induced temperature jump in water. *Appl Phys B* 74(1):57–66.
- Agno M, Frontali C (1967) Viscosity measurements of alcohol–water mixtures and the structure of water. *Proc Natl Acad Sci USA* 57(4):856–860.
- Bakker JM, et al. (2008) Tautomerism of uracil probed via infrared spectroscopy of singly hydrated protonated uracil. *J Phys Chem A* 112(48):12393–12400.
- Chang KC, Grunwald E (1976) Water participation in proton-transfer reactions of glycine and glycine methyl ester. *J Phys Chem* 80(13):1422–1425.
- Pérez A, Tuckerman ME, Hjalmarson HP, von Lilienfeld OA (2010) Enol tautomers of Watson–Crick base pair models are metastable because of nuclear quantum effects. *J Am Chem Soc* 132(33):11510–11515.
- Nesmeyanov AN, Zavelovich EB, Babin VN, Kochetkova NS, Fedin EI (1975) 1H and 13C NMR study of tautomerism in azoles—I: Proton transfer in the absence of solvation. *Tetrahedron* 31(11–12):1461–1462.
- Ahrens ML (1973) Proton transfer kinetics of 5'-deoxyuridoxal. *Biochim Biophys Acta Gen Subj* 320(1):86–96.
- Chang K-C, Grunwald E (1976) Bifunctional proton transfer of the conjugate base of uracil compared with that of imidazole in aqueous solution. *J Am Chem Soc* 98(12):3737–3738.
- Eigen M, Hammes GG, Kustin K (1960) Fast reactions of imidazole studied with relaxation spectrometry. *J Am Chem Soc* 82(13):3482–3483.
- Chevrier M, Guillerez J, Dubois JE (1983) Equilibrium and activation thermodynamic parameters of the tautomerism of 6-methoxy-2-pyridone in water. *J Chem Soc Perkin Trans 2* (7):979–982.